Proceedings of the Eighth Meeting of the International Collaboration on Advanced Neutron Sources (ICANS-VIII)
8-12 July 1985, Rutherford Appleton Laboratory Report RAL-85-110

DESIGN OF THE LOW-Q DIFFRACTOMETER AT LOS ALAMOS

P. A. Seeger, A. Williams, and J. Trewhella
Los Alamos National Laboratory, Los Alamos, NM 87545, U.S.A.

Abstract

Instrument criteria are presented for the Low-Q Diffractometer (LQD) at the Los Alamos Neutron Scattering Center (LANSCE), and a design is developed to meet these criteria. The collimator consists of multiple-aperture pinhole plates, and incorporates "dynamic gravity focusing" to center all wavelengths on the detector. Monte-Carlo simulations are used to test and optimize the design. Analysis of these simulations required development of some of the data-reduction software which will be used to convert experimental histograms vs. radius and time to I(Q) data.

1. Introduction

The Low-Q Diffractometer (LQD) for the Los Alamos Neutron Scattering Center (LANSCE) will be installed on flight path 10 (the northeast corner) in the existing Weapons Neutron Research (WNR) experimental hall. With the Proton Storage Ring (PSR) operating at 24 Hz, the proposed total flight path of 12.5 m allows use of neutron wavelengths out to 13 Å before frame overlap, without the need for choppers or filters. The general floor plan is shown in fig. 1.

This flight path views a liquid hydrogen moderator which should produce the same neutron spectrum as the SNS liquid hydrogen moderator. The measured spectrum [1] is shown in an equal-area plot (i.e., number of neutrons proportional to area anywhere on the plot) in fig. 2 (solid line). There is a peak at 14 meV (2.4 Å wavelength) due to the transparency of para-hydrogen, and the long-wavelength data (measured to 10 Å or 0.8 meV) fit a Maxwellian of effective temperature 2.1 meV. We have arbitrarily

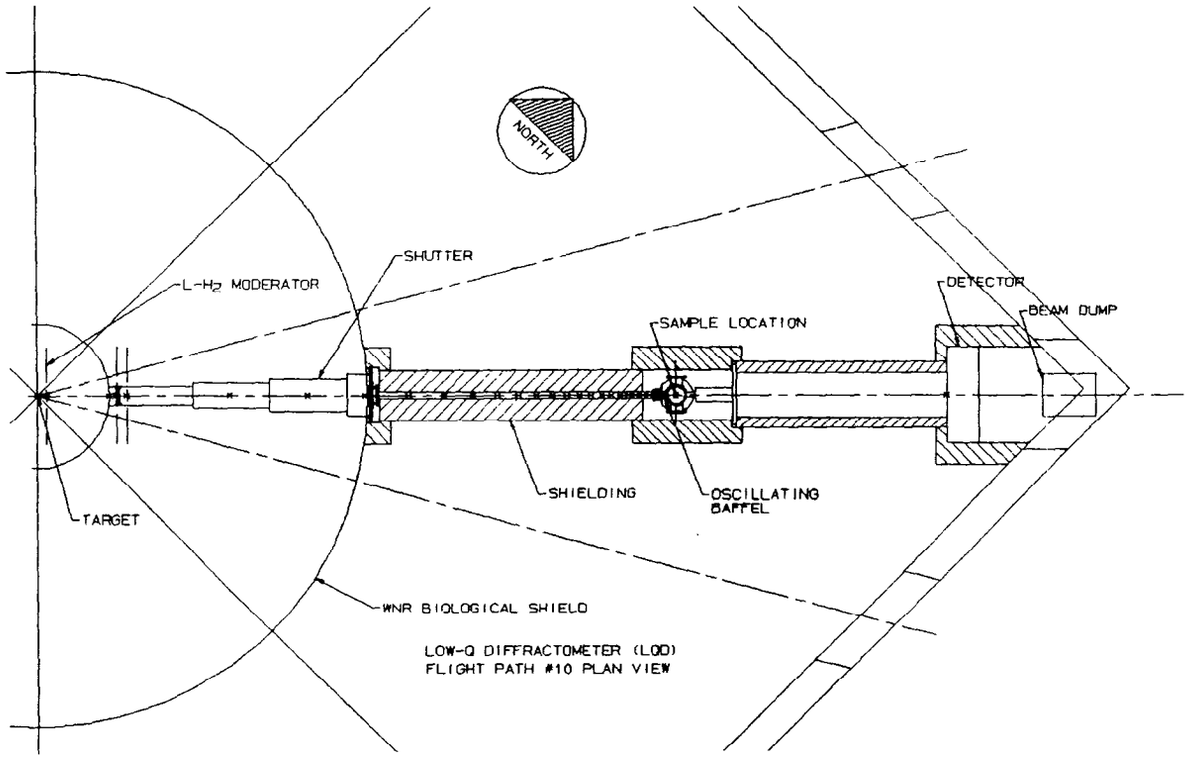

Fig. 1. Floor plan of the proposed LQD, at flight path 10 of LANSCE.

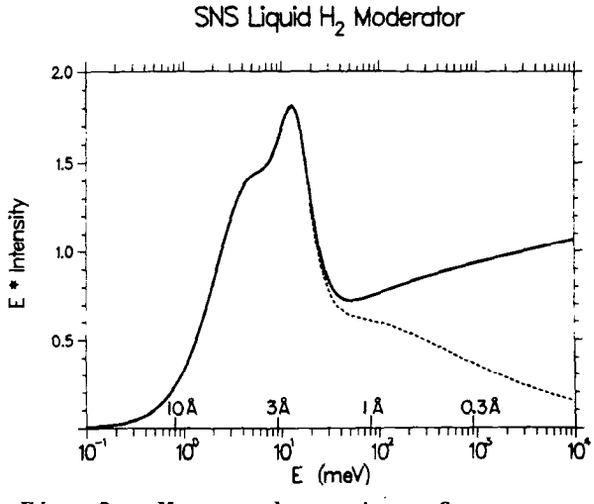

Fig. 2. Measured spectrum from the liquid hydrogen moderator at SNS.

chosen λ = 8 Å, at which the intensity is about a quarter maximum, to represent the maximum wavelength for obtaining statistically significant results when estimating the low-Q limit of the instrument.

The detector resolution and efficiency are assumed to be good enough not to affect optimization. For instance, the Anger camera [2,3] is recorded in bins 2.3 mm square, and it has an rms resolution better than 1.5 mm. This will not contribute significantly to the resolution if the sample-to-detector distance L_2 > 2.5 m. Efficiency affects the short-wavelength/high-Q end of the spectrum; the dashed line in fig. 2 illustrates the effective spectrum for a 1/v detector equivalent to a 2-mm thickness of ^{6}Li glass scintillator. At 0.3 Å, the efficiency is 39%.

2. Design Criteria

The primary requirement of the instrument is to be able to take statistically significant data at a minimum momentum transfer $Q_{min} = 0.003\ \text{Å}^{-1}$. With $\lambda_{max} = 8$ Å,

$$\theta_{min} = \frac{\lambda_{max} Q_{min}}{2\pi} = 3.8 \text{ mrad} \qquad (1)$$

We also require an rms resolution at least as good as 30% at Q_{min}, so that the standard deviation of θ must be

$$\sigma_\theta < 1.15 \text{ mrad.} \qquad (2)$$

These angular criteria will establish the relative sizes of the collimator apertures, and will be developed more fully in the next section.

An obvious design goal is to maximize the counting rate of an experiment. Once the angular parameters are determined, however, there is very little which can be done to affect the flux on sample [4]; for instance, if the instrument is shortened to gain flux by the $1/R^2$ increase of solid angle, then the area of moderator seen at any point on the sample must be decreased by exactly the same factor to maintain resolution. For a given moderator surface brightness ($n/cm^2/ster/s$), the only way to increase intensity is by increasing the sample size, up to the limit that the full moderator surface is being used. Since frame overlap (as well as the available space in the experimental hall) limits the scale factor by which the design can be multiplied, the only way to increase sample size is through use of multiple-aperture collimators.

The third criterion is to allow an extended dynamic range in Q, up to at least $1.0\ \text{Å}^{-1}$. This is readily accomplished by utilizing a wide band of the wavelength range of the pulsed source, and by using an area detector covering a reasonably large angular range. Since we wish to record all wavelengths longer than 0.3 Å, a chopper to block the power pulse is impractical. If located 4.5 m from the source, it would have to be fully open within 320 μs after the proton pulse. Since the beam diameter is about 80 mm at that location, the linear velocity would be 250 m/s and the diameter would be 3.3 m. We will rely on time of flight to eliminate the power pulse; the detector and associated electronics must recover fully within a few hundreds of μs.

3. Collimator Aperture Sizes

The variance of the scattering angle, θ, due to moderator and sample collimation is [5]

$$V[\theta] = \frac{1}{2L_1^2}\overline{r_1^2} + \frac{1}{2}\left(\frac{1}{L_1} + \frac{1}{L_2}\right)^2 \overline{r_2^2} \quad , \tag{3}$$

where r_1 and r_2 are axial displacements on the moderator and sample, respectively, and the path lengths are as shown in fig. 3. In all previous studies [5-7], the distances ℓ_1 and ℓ_2 were assumed to be small, and the radii of the moderator and sample were assumed to be equal to the aperture radii, R_1 and R_2. At the recommendation of our design review committee [8], we now propose that ℓ_1 be relatively large so that we will have the versatility of changing the collimator system without changing anything inside the biological shield. The effect of ℓ_1 and ℓ_2 on aperture optimization must be re-examined.

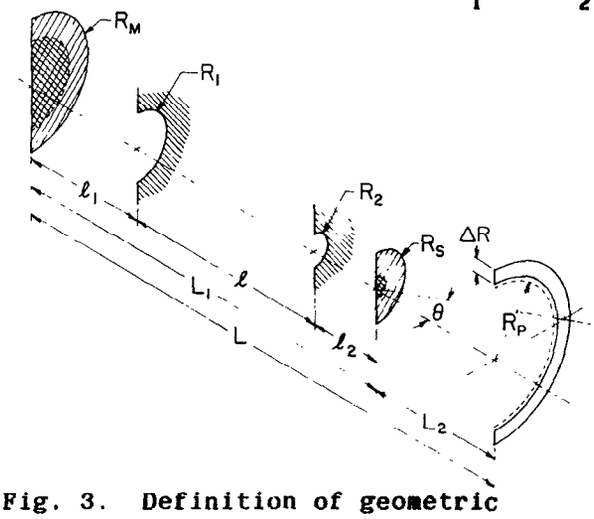

Fig. 3. Definition of geometric parameters.

From the development of either [5] or [6], the two terms in eq. (3) should be made equal. Thus

$$\overline{r_1^2} \,/\, \overline{r_2^2} = \left(\frac{L_1 + L_2}{L_2}\right)^2 \quad , \tag{4}$$

or the root-mean-square radii are proportional to distances from the detector. The distribution of r_1^2 is constant out to the radius of the umbra, $R_1 + (R_1 - R_2)\ell_1/\ell$, and falls to zero at the penumbra radius, $R_M = R_1 + (R_1 + R_2)\ell_1/\ell$. Thus r_1^2 depends on both R_1 and R_2 (as does r_2^2), but the arithmetic average of the umbra and penumbra radii is $R_1(1+\ell_1/2\ell)$.

We now choose path lengths based on practical considerations, and hunt for aperture sizes which satisfy eqns. (1), (2), and (4). If necessary, we can then modify the path lengths and iterate. For L_1 = 8.75 m and L_2 = 3.75 m, we require

$$\overline{r_2^2} \,/\, \overline{r_1^2} = (0.30)^2 \tag{5}$$

Assuming ℓ_1 = 4.75 m, ℓ_2 = 0.25 m, and ℓ = 3.75 m, a simple Monte-Carlo code was run and the radii adjusted until the ratio converged at

$$R_2/R_1 = 0.55, \tag{6}$$

which is about 8% larger than it would be if the aperture radii (instead of the rms radii) converged to the detector. The penumbra radius at the detector,

$$R_P = R_2 + \frac{R_1+R_2}{\ell}(L_2+\ell_2) = 3.99\ R_2\ , \tag{7}$$

must be chosen to satisfy eq. (1). Allowing a 1 mm safety margin, and taking ΔR = 2.3 mm,

$$\theta_{min} = (R_P + 1\ \text{mm} + \Delta R/2)/L_2 \tag{8}$$

$$R_P < 12.1\ \text{mm} \tag{9}$$

$$R_1 = 5.47\ \text{mm}, \quad R_2 = 3.03\ \text{mm} \tag{10}$$

The standard deviation of θ (square root of eq. (3)) is then 0.81 mrad, well within eq. (2). The penumbra radii at the moderator and sample are

$$R_M = 16.2\ \text{mm}, \quad R_S = 3.6\ \text{mm} \tag{11}$$

4. Multiple Apertures

The moderator and sample sizes in eq. (11) do not take good advantage of the available source. Multiple aperture sets, all converging to the same point at the detector, increase the intensity without affecting the resolution. The pattern of 19 holes shown in fig. 4 matches the size of the moderator (120 mm x 120 mm) and illuminates a sample 36 mm in diameter.

Intermediate beam scraping baffles are required to prevent neutrons crossing from one imaginary tube to another in the multiaperture system. The holes in these baffles should be large enough not to intercept the actual beam, and must be further enlarged to account for the different parabolic trajectories followed through the collimator by neutrons of different velocities (because of gravity, the neutrons do not follow straight lines; see the following section). Twelve baffles will be required, with variable spacing; they become quite close as the size of holes relative to their spacing increases.

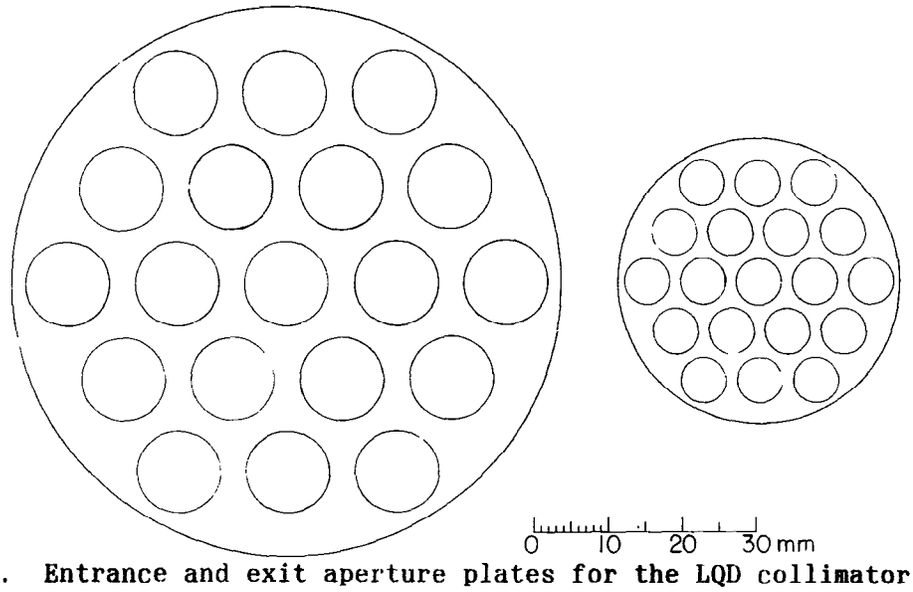

Fig. 4. Entrance and exit aperture plates for the LQD collimator. Each corresponding pair of holes defines a beam with appropriate divergence, and all converge to the same point at the detector. Intermediate baffles prevent crosstalk between beams.

In the limit that the holes cover the entire area of the baffles, the collimators are continuous and take the form of converging Sollers. We considered three possible geometries: concentric converging cones, an array of converging hexagonal pyramids, and conventional alternating horizontal and vertical Soller slits. However all systems involving extended surfaces were rejected because of "mirror reflection" of long wavelength neutrons from any surface [9]. In fig. 5 we show the reflection probability for 8-Å neutrons as a function of glancing angle, from three different substances. For absorbing surfaces, the effective index of refraction is complex and there is no critical reflection angle (as there is for Cu). But the probability always goes to unity as the angle goes to zero, and reflection at angles comparable to our required collimation is far from negligible. The situation is improved if the surfaces are rough, but there will always be some halo always be some halo on the beam, requiring a larger beam stop and hence larger θ_{min}. Also note that the reflection probability is proportional to λ^2, so the effect is most damaging at the smallest values of Q.

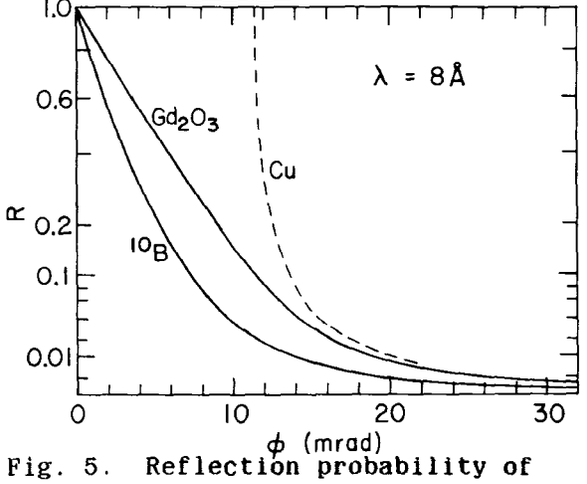

Fig. 5. Reflection probability of 8 Å neutrons.

5. Dynamic Gravity Focusing

At 24 Hz, neutrons recorded at the end of the frame will have fallen 8.50 mm under the influence of gravity, compared to where they were pointed when they left the moderator. (Gravity is smaller at LANSCE than at any other source represented in ICANS, because of our lower latitude and higher altitude.) To minimize the size of the beam stop we want to choose neutrons whose trajectories strike the detector at its center; fig. 6 shows the parabolic trajectories of two neutrons with different horizontal velocity. If we replace the horizontal velocity by $h/m\lambda$, and use y_o and v_o to represent the initial position and vertical velocity of the neutron, then

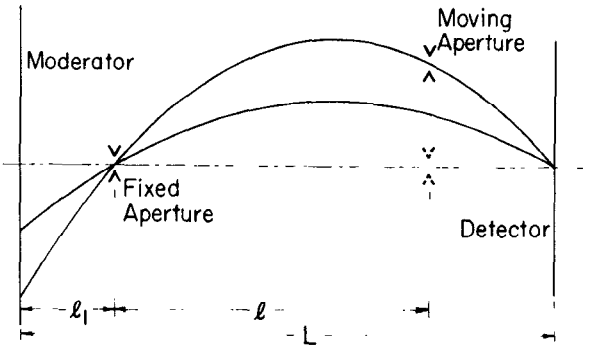

Fig. 6. Dynamic gravity focusing.

$$y = y_o + \frac{m}{h}\lambda\, v_o\, x - \frac{1}{2} g \left(\frac{m}{h}\lambda\right)^2 x^2 \ . \tag{12}$$

If the entrance aperture and the detector center are taken as fixed points, so that $y = 0$ at $x = \ell_1$ and at $x = L$, then

$$y = \frac{1}{2} g \left(\frac{m}{h}\lambda\right)^2 [-\ell_1 L + (\ell_1 + L)\, x - x^2] \tag{13}$$

The exit aperture of the collimator, at $x = (\ell_1 + \ell)$, must move vertically in phase with the beam. Neutrons of wavelength λ arrive at the moving aperture at $t = (\ell_1 + \ell)m\lambda/h$, and the required motion is

$$y = \frac{1}{2} g \left(\frac{L}{\ell_1 + \ell} - 1\right) \left(1 - \frac{\ell_1}{\ell_1 + \ell}\right) t^2 \tag{14}$$

For the flight paths chosen for the LQD, this becomes

$$y = (1.016\ \text{m-s}^{-2})\ t^2 \ , \tag{15}$$

and the maximum excursion (for 13 Å neutrons) is 0.82 mm. Without correction, the droop at the detector would be 1.69 mm. This correction has become much smaller than our original estimates, because ℓ_1 is much larger. If we return to the design with $\ell_1 = 1.00$ m, the maximum excursion is

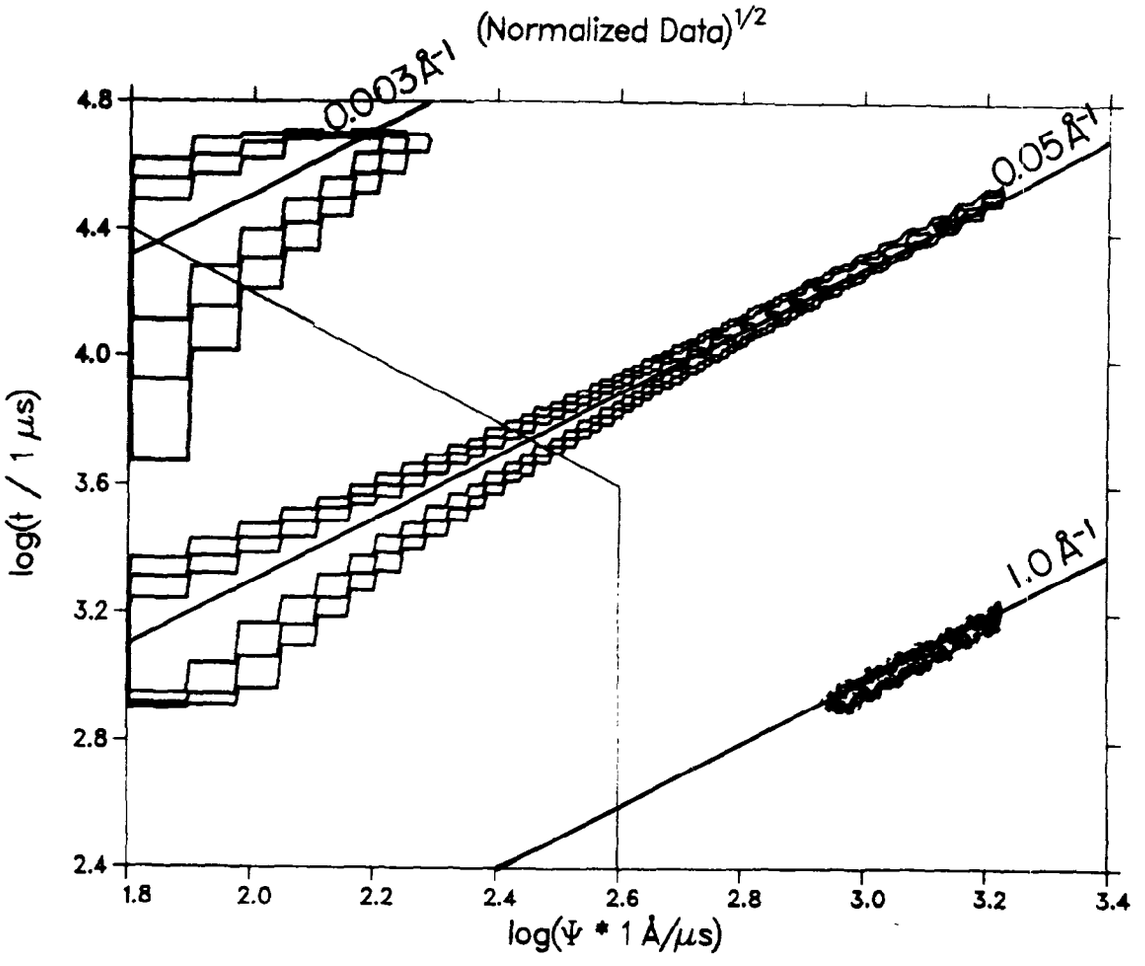

Fig. 7. Simulated data for scattering at three values of Q. Ψ represents the radial coordinate on the detector, and t is a measure of neutron wavelength. Data have been normalized to the incident spectrum.

1.63 mm, to correct for a droop of 2.50 mm. Whether or not the dynamic correction is made, eq. (13) must be used to compute sizes and elevations of the intermediate baffles in the system.

6. Monte-Carlo Simulations

The various collimator systems were run through Monte-Carlo simulations to estimate the resolution. Details are given in ref. [7]. Two forms of perfect scatterers were considered: either every neutron was scattered with exactly the same magnitude of the momentum transfer (δ-function Q), or else the scattering law was that of non-interacting hard spheres of uniform radius. Neutrons reaching the detector were binned vs. radius and time, with the radial bins 3.0 mm wide and logarithmic time bins of width

$\Delta t = t/600$. Normalized contour plots of three constant-Q runs are given in fig. 7. The radial variable has been converted to

$$\Psi = \frac{4\pi\, m\, L}{h} \sin(\theta/2), \tag{16}$$

so that

$$Q = \Psi/t \tag{17}$$

and a line of constant Q is a straight line with slope +1 on the log-log plot.

The histogram bins are wide in the Ψ direction (especially at small Ψ) and very short in t, as shown in fig. 8. A Q bin is a diagonal band, which includes contributions from many Ψ-t bins. Our binning procedure is to take t equal to the mid-value of the bin, and to compute the fraction of each log(Ψ) bin which falls within the Q bin. We then take the <u>average</u> of the <u>normalized</u> count rate from each contributing old bin weighted inversely as its variance. All position and/or time dependent corrections <u>must</u> be performed <u>before</u> rebinning. The weighted average may then be multiplied by the area of the new bin to produce an "intensity."

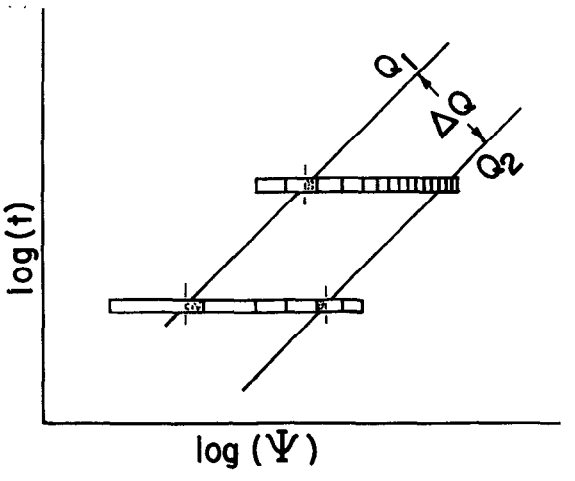

Fig. 8. Relationship of Q bins to Ψ and t bins.

Fig. 9 shows the resulting intensity vs. Q when <u>all</u> data are summed. (Note that a square-root scale is used to emphasize the tails of the distributions.) Comparing to fig. 7, it is clear that the long tails in fig. 9 result from including short wavelength data from the innermost annuli of the detector, where the resolution is poor. If we omit data in the lower-left corner of fig. 7, the result is fig. 10. On this figure, I is the fraction of all detected neutrons which is retained. Note the greatly improved standard deviations, σ.

The same data-reduction procedure was applied to the hard-sphere simulations. We have also used a fitting program for spheres and a Guinier analysis program, both including propagation of errors, to investigate the statistical precision which may be obtained. The resulting intensity distributions and fitted parameters are shown for the case of R = 30 A in fig. 11. With the source operating at 100 μA, and a 1% scattering sample, the data-collection time for this number of neutrons would be less than 1 s.

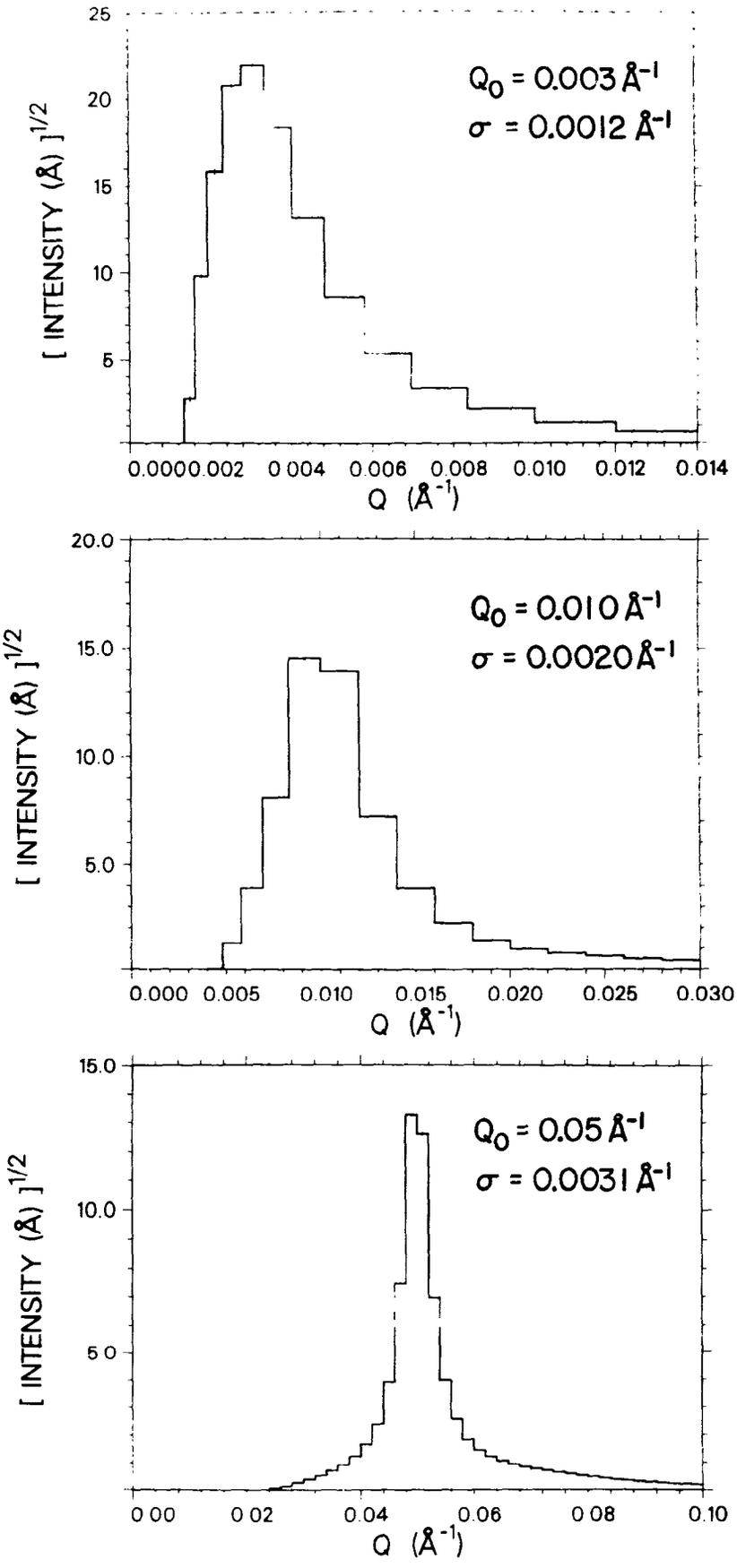

Fig. 9. Sum of data of all wavelengths, for three constant Q simulations.

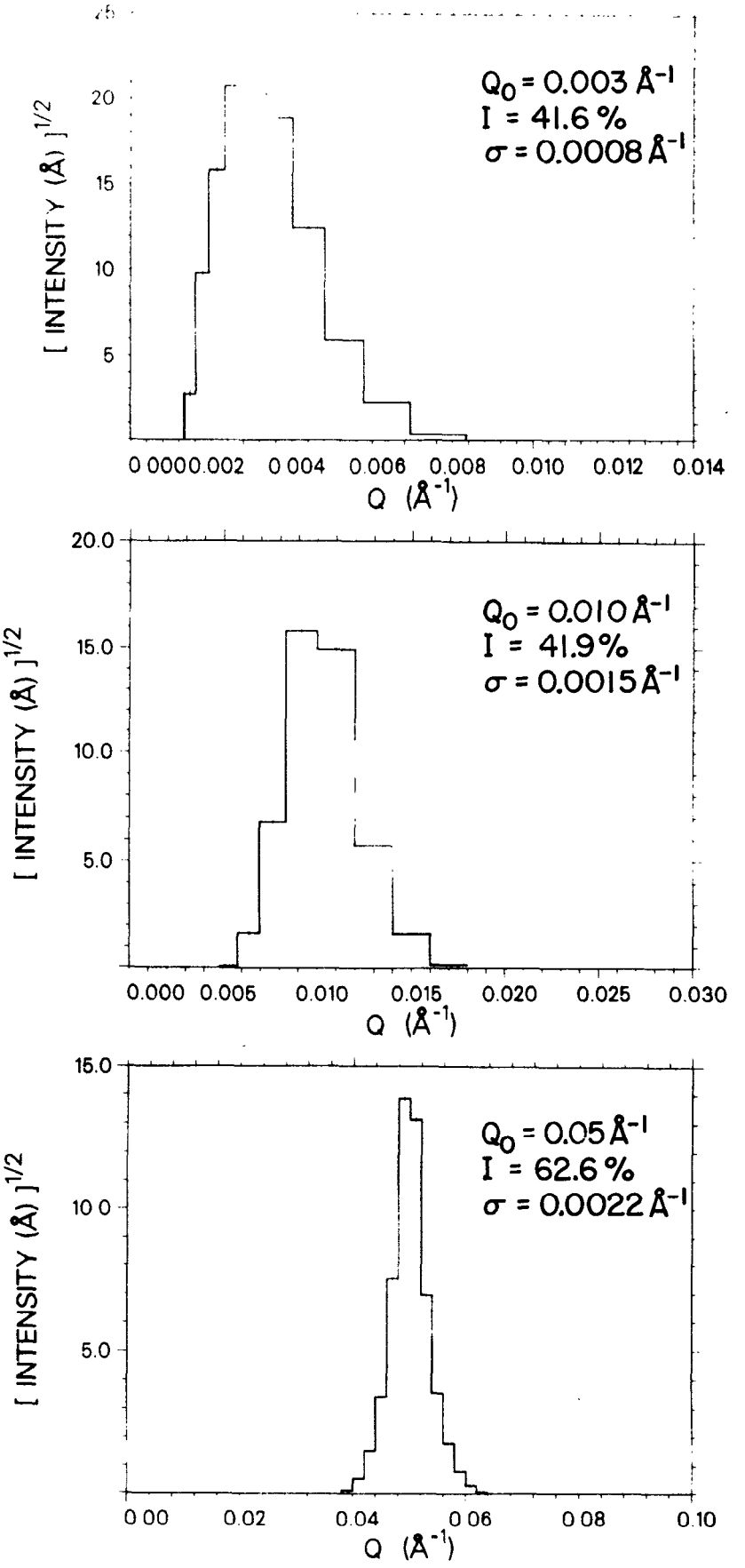

Fig. 10. Sum of data, excluding lower-left corner from fig. 7.

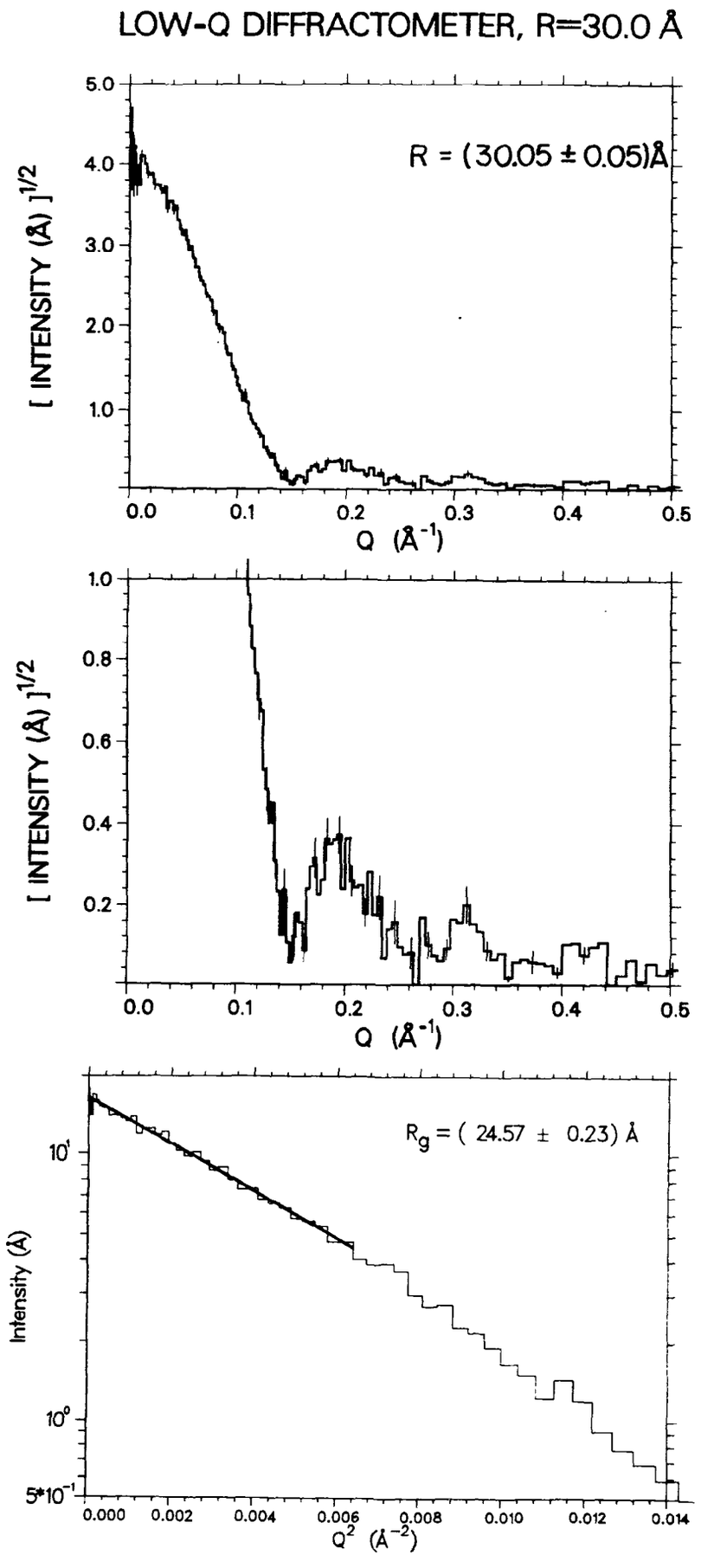

Fig. 11. Simulated data for hard sphere scattering with R = 30 Å.

A significant feature of the LQD is that a broad range of Q is measured in a single experiment without any collimation or detector changes. This will allow high prescision model fits in the range of sizes from 10 to 300 Å to be obtained in slightly less time than at D-11. On the other hand, to obtain the same precision as D-11 for a Guinear fit will require about four time as long.

Acknowledgments

This work was permformed under the auspices of the U.S. Department of Energy, Office of Basic Energy Sciences.

References

[1] T.D. Perring, A.D. Taylor, and D.R. Perry, Rutherford Appleton Laboratory report RAL-85-029 (1985).

[2] P.A. Seeger, I.E.E.E. Trans. Nucl. Sci. **NS31** (1984) 274.

[3] P.A. Seeger and M.J. Nutter, this conference (1985).

[4] P.A. Seeger, Proceedings of the International Neutron Scattering Conference, Santa Fe, August (1985).

[5] P.A. Seeger, Nucl. Instr. and Meth. **178** (1980) 157.

[6] D.F.R. Mildner and J.M. Carpenter, J. Appl. Cryst. **17** (1984) 24.

[7] P.A. Seeger and R. Pynn, submitted to Nucl. Instr. and Meth. (1985).

[8] Committee members were J.M. Carpenter, J.E. Epperson, J.B. Hayter, R.Pynn, K. Rhyne, J.M. Rowe (chair), D. Schaefer, and J.W. White.

[9] I.I. Gurevich and L.V. Tarasov, "Low-Energy Neutron Physics" (North-Holland, Amsterdam, 1968) p. 58.